Heliyon 10 (2024) e39025

Contents lists available at ScienceDirect

Heliyon

journal homepage: www.cell.com/heliyon

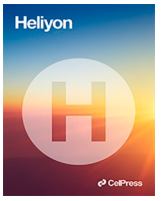

Research article

An immune-related gene pair signature predicts the prognosis and immunotherapeutic response in glioblastoma

Gang Wang [a,c], Yingchun Man [b], Kui Cao [a], Lihong Zhao [a], Lixin Lun [a], Yiyang Chen [a], Xinyu Zhao [a], Xueying Wang [a], Lijie Zhang [b,*], Chuncheng Hao [a,**]

[a] Department of Head and Neck Radiation Oncology, Harbin Medical University Cancer Hospital, Harbin, China
[b] Department of Medical Oncology, Beidahuang Industry Group General Hospital, Harbin, China
[c] Department of Radiation Oncology, Cancer Hospital, Chinese Academy of Medical Sciences and Peking Union Medical College, Beijing, China

ARTICLE INFO

Keywords:
Glioblastoma (GBM)
IRGP
Prognostic model
Immune infiltration
Immune checkpoints

ABSTRACT

Background: Glioblastoma (GBM) has the feature of aggressive growth and high rates of recurrence. Immunotherapy was not included in standard therapy for GBM due to lacking the predictive biomarkers. In the present study, we performed an immune-related gene pair (IRGP) signature to predict the prognosis and immunotherapy response of GBM.
Methods: A total of 160 GBM patients from TCGA were included. ssGSEA was conducted to evaluate the immune infiltration level. Univariate Cox, LASSO regression analysis, ROC analysis, and Kaplan-Meier survival analysis were applied to construct and evaluate the risk model. Moreover, the association between immune infiltration and the risk score was assessed. Finally, the expression of immune checkpoints between different risk groups was explored.
Results: According to the normal/tumor, high-/low-immunity group, we identified 125 differentially expressed immune-related genes. Subsequently, a prognostic model including 22 IRGPs was established. The area under the ROC curve to predict 1, 3, and 5-year was 0.811, 0.958, and 0.99 respectively. According to the optimal cut-off value of the 3-year ROC curve, patients were classified into high- and low-risk groups. The Kaplan-Meier analysis result indicated that patients in the low-risk group have longer survival time. The risk score was an independent prognostic predictor ($P < 0.001$). Moreover, *PDCD1* was positively correlated with the risk score ($P < 0.01$). We also found that patients with high *PDCD1* expression had worse survival.
Conclusions: The IRGP signature was built to predict the prognosis of GBM patients. This signature can serve as a tool to predict the response to immunotherapy in GBM.

1. Introduction

Glioblastoma (GBM) is a kind of typical malignant primary brain tumor in adults [1]. Because of its high invasiveness and lethality, the median overall survival of newly diagnosed GBM cases is only approximately 15 months [2,3]. Despite initial treatment with maximal surgical resection followed by chemoradiotherapy, most of the cases still relapse within approximately 2 cm around the tumor cavity 6–9 months after treatment [4]. Hence, its five-year survival rate is very low, at about 6.8 % [5]. Moreover, GBM has

* Corresponding author. No. 235 Hashuang Road, 150088, Harbin, China.
** Corresponding author. No. 150 Haping Road, 150000, Harbin, China.
E-mail addresses: zlj870502@163.com (L. Zhang), haocc@hrbmu.edu.cn (C. Hao).

https://doi.org/10.1016/j.heliyon.2024.e39025
Received 21 June 2024; Received in revised form 2 October 2024; Accepted 4 October 2024
Available online 5 October 2024

different molecular characteristics and subtypes, and the same treatment model may lead to different clinical outcomes [6]. Therefore, patients are needed be more accurately stratified to develop the optimal treatment.

Programmed death-1 (PD-1) is a cell surface receptor expressed on a variety of immune cells [7]. The programmed death-ligand 1 (PD-L1) is overexpressed on the surface of malignant tumor cells. The binding of PD-1 to its ligand PD-L1 activates the downstream pathways and causes the immune evasion of tumors [8]. The inhibitors targeting PD1 and PDL1 exert significant antitumor effects by restoring the killing effects of immune cells and avoiding immune escape [9] and have shown significant efficacy in many tumors, like melanoma [10] and NSCLC [11]. Nevertheless, it failed to demonstrate the expected benefit of GBM [12–14], which may be related to the inability to identify specific cases that would benefit from immunotherapy [14]. PD-L1 is an important biomarker for predicting the effect of immunotherapy. Some scholars found that PD-L1 is related to poor prognosis in GBM [15], while others showed inconsistent results [16]. Due to these contradictory results, it is necessary to combine other markers to identify cases that are suitable for immunotherapy.

Some models based on gene expression characteristics have been constructed to identify such specific patients [17,18]. In GBM studies, most of the models are based on a single gene [19,20] or different phenotypes, such as inflammation [21], cuproptosis [22], immune response, oxidative stress [23], and cellular senescence [24]. They were constructed based on the exact expression level of genes, which are easily affected by individual variations. In this study, we utilized pairwise comparison and score calculation to construct an IRGP signature. This method utilized the relative ranking of gene expression levels and did not need the normalization of data. Then, we explored the diagnostic and prognostic value of the IRGP signature. The association between the immunological parameters and the signature was also explored. Subsequently, GSEA was applied to investigate the specific mechanisms of the signature.

2. Methods

2.1. Data acquisition and differentially expressed analysis

The transcriptome profiling data of 160 GBM patients containing clinical data was obtained from TCGA. Cases with a survival time of less than one month were excluded. An immune gene chip was downloaded from the MSigDB database (http://software.broadinstitute.org/gsea/downloads.jsp). The ssGSEA was applied to evaluate the types of immune cells and infiltration level with the GSVA (version 1.34.0) and GSEABase (version 1.67.0) packages of R. Through clustering analysis, the GBM cases were divided into high- and low-immunity groups according to their immune infiltration levels with the sparcl package of R (version 1.0.4–1). Differential expression analysis was carried out in two immunity groups (log2-fold change (FC) $>$ 1, FDR $<$0.05), as well as between tumor and normal samples (log2-FC$>$1.5, FDR$<$0.05). Differentially expressed immune-related genes (DEIRGs) were obtained with the venn diagram package of R (version 1.7.3).

2.2. Pairing DEIRGs

The method of constructing the model has been previously reported [25]. In short, we first performed the pairwise comparison in all samples. In each sample, if the expression of the first gene was higher, it was labeled as 1, or else as 0. The score of every IRGP was computed. Hence, the condition of the IRGP score included in the model is its frequency value in a range of 20 % and 80 % of all samples.

2.3. Establishment of an IRGP risk model

Univariate Cox method was applied to identify the prognostically relevant IRGPs based on the survival package of R (version 3.3.1) ($P < 0.01$). Next, LASSO Cox regression was conducted to further filter meaning IRGPs with the glmnet package of R (version 3.0–2) [26]. The LASSO regression was iterated for 1000 cycles. Ultimately, a total of 22 IRGPs were identified, and the risk score was determined as follows: RiskScore = score of DEIRG pairs 1 x β1 DEIRG pairs 1+ … …+ score of DEIRG pairs n x βn DEIRG pairs n. The optimal cutoff value of the riskscore was calculated according to the 3-year ROC curve via the survivalROC package of R (version 1.0.3) [27]. Then cases were divided into high- and low-risk groups.

2.4. Validation of the established risk model

Kaplan-Meier approach was used to explore the prognostic significance of the risk score with the survival and survminer (version 0.4.9) packages of R. We also investigated the relation between the riskscore and clinicopathological factors. Univariate and multivariate Cox analyses were conducted to confirm the predictive ability of the riskscore. A nomograph was developed to predict survival probability with the rms package of R (version 6.3–0).

2.5. Estimation of immune infiltration

The immune infiltration status was analyzed using TIMER, CIBERSORT, XCELL, and EPIC. The Spearman analysis was applied to analyze the association between the risk score and the immune cell infiltration ($P < 0.05$).

2.6. Exploration of immune checkpoint molecular expression

We applied the ggplot2 package of R and the Wilcoxon test to explore the expression of immune checkpoint molecules between two risk groups.

2.7. Gene set enrichment analyses (GSEA)

GSEA software (version 4.0.1) was applied to conduct GSEA between two risk groups. Identified the enriched terms in KEGG and Hallmarks in two groups. $P < 0.05$ and FDR <0.05 were used as the selection criteria.

2.8. Statistical analysis

We performed statistical analyses based on R software (version 4.0.3, Vienna, Austria). The log-rank test was applied to compare the survival time in different risk groups. The Cox regression method was used to assess the prognostic role of the risk model. Spearman test was applied for correlation analyses. Statistical significance was defined as $P < 0.05$ unless specified otherwise.

3. Results

3.1. Identification of DEIRGs

The flowchart of this study is exhibited in Fig. 1. The transcriptome profiling data of GBM including 5 normal and 160 tumor samples were downloaded from TCGA. Subsequently, the tumor samples were subjected to ssGSEA based on immune gene sequence, followed by clustering analysis to divide them into high- and low-immunity groups according to the immune enrichment scores (Fig. 2A). The distinct difference in immune enrichment scores was depicted through a heat map and PCA diagram (Fig. 2B and C). Further differential analysis identified 257 immune-related genes with significant differences in two groups (Fig. 2D) (log2FC > 1, FDR<0.05). Additionally, 4736 differentially expressed genes between tumor and normal samples were identified (log2FC > 1.5, FDR<0.05) (Fig. 2E). By intersecting these two datasets, we identified 125 DEIRGs for further analysis (Fig. 2F).

3.2. Establishment of an IRGP risk model

The 125 DEIRGs were transformed into gene pairs by iteration loop and a 0-or-1 matrix screening, a total of 2893 IRGPs were identified. These IRGPs were included in univariate Cox model ($P < 0.01$), and 57 IRGPs related to prognosis were obtained. Next, these prognostic IRGPs were subjected to LASSO Cox analysis (Fig. 3A and B). Ultimately, 22 IRGPs consisting of 36 genes (Table 1) were identified to construct the risk model. The risk score can be determined according to the coefficients of selected IRGPs.

Next, we conducted the time-dependent ROC curve analysis of the risk model. The AUC was 0.811, 0.958, and 0.99 for 1, 3, and 5-year respectively (Fig. 3C). However, due to the limited number of GBM patients surviving beyond 5 years in the TCGA dataset, there

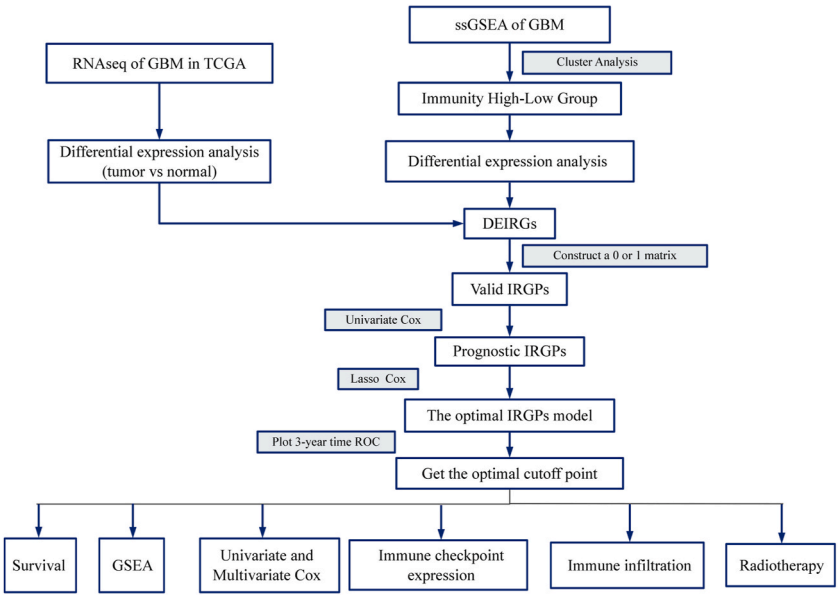

Fig. 1. Study flow chart.

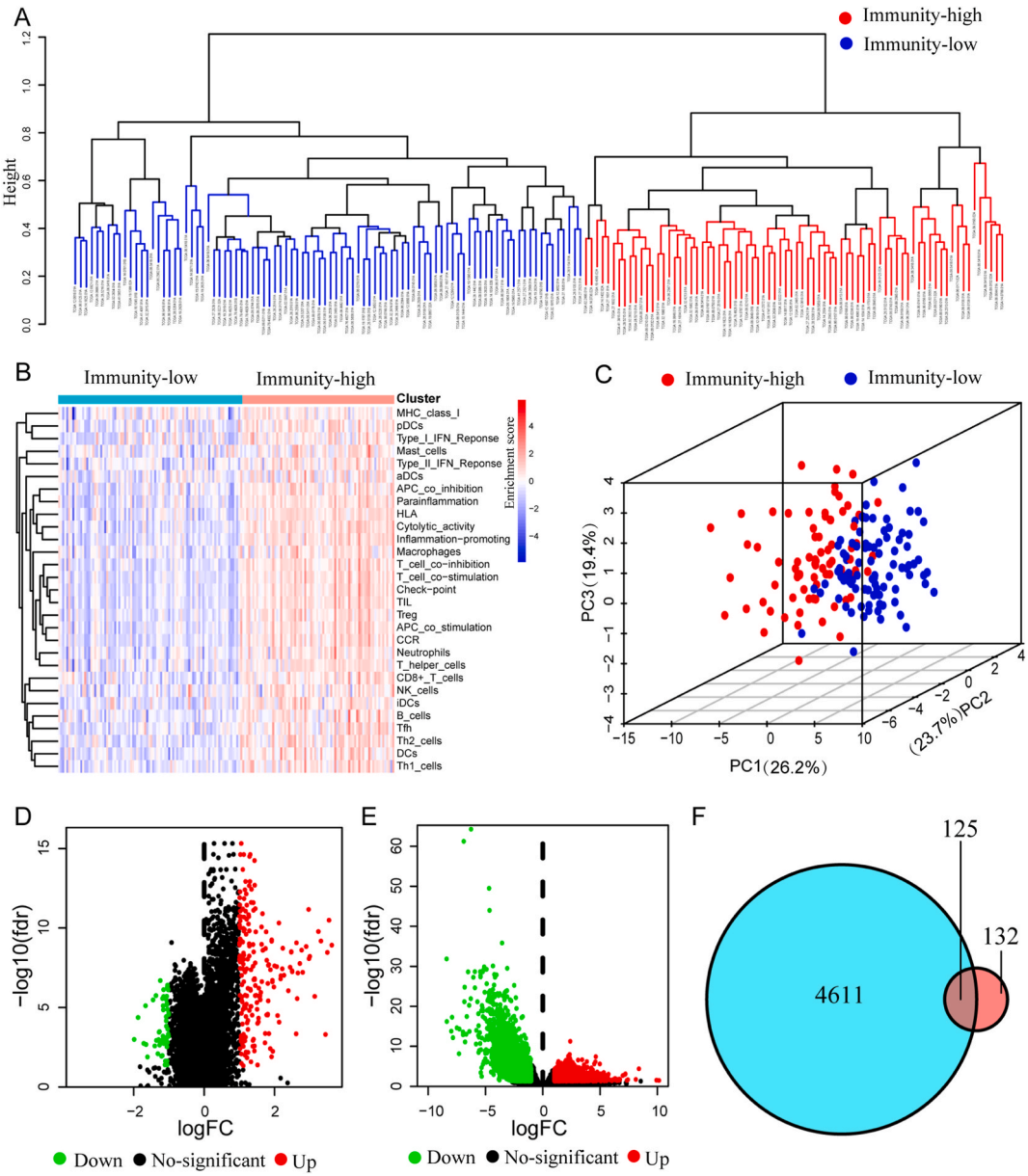

Fig. 2. Identification of differentially expressed immune-related genes (DEIRGs) using TCGA dataset. (A) Hierarchical clustering of patients with GBM based on ssGSEA, with each branch representing a sample, height in the vertical coordinate being the clustering distance, and the horizontal coordinate being the grouping information. (Red: high immunity group, blue: low immunity group). (B) The enrichment levels of 29 immune-related cells and types in the high- and low-immunity groups. (C) Principal component analysis (PCA) plot of the distribution status of the high- and low-immunity groups. (D) Volcano plot of differential expression analysis between high- and low-immunity groups. (E) Volcano plot of differential expression analysis between tumor and normal samples. (F) The Venn Diagram of two gene sets.

may be potential bias in predicting the 5-year OS using this model. Next, based on the 3-year ROC curve, cases were classified into high- and low-risk groups according to the optimal cut-off value (Fig. 3D and E). It is worth noting that the risk score is negatively related to the survival time and positively related to the mortality rate (Fig. 3F).

3.3. Association in risk model and clinical features

The Kaplan-Meier result suggested that cases in the high-risk group exhibited poor prognosis ($P < 0.001$) (Fig. 4A). Next, Wilcoxon tests were used to investigate the relation between the risk score and clinical factors. It was found that when compared with patients without radiotherapy, patients treated with radiotherapy had lower risk scores (Fig. 4B). Nevertheless, there exists no difference in the

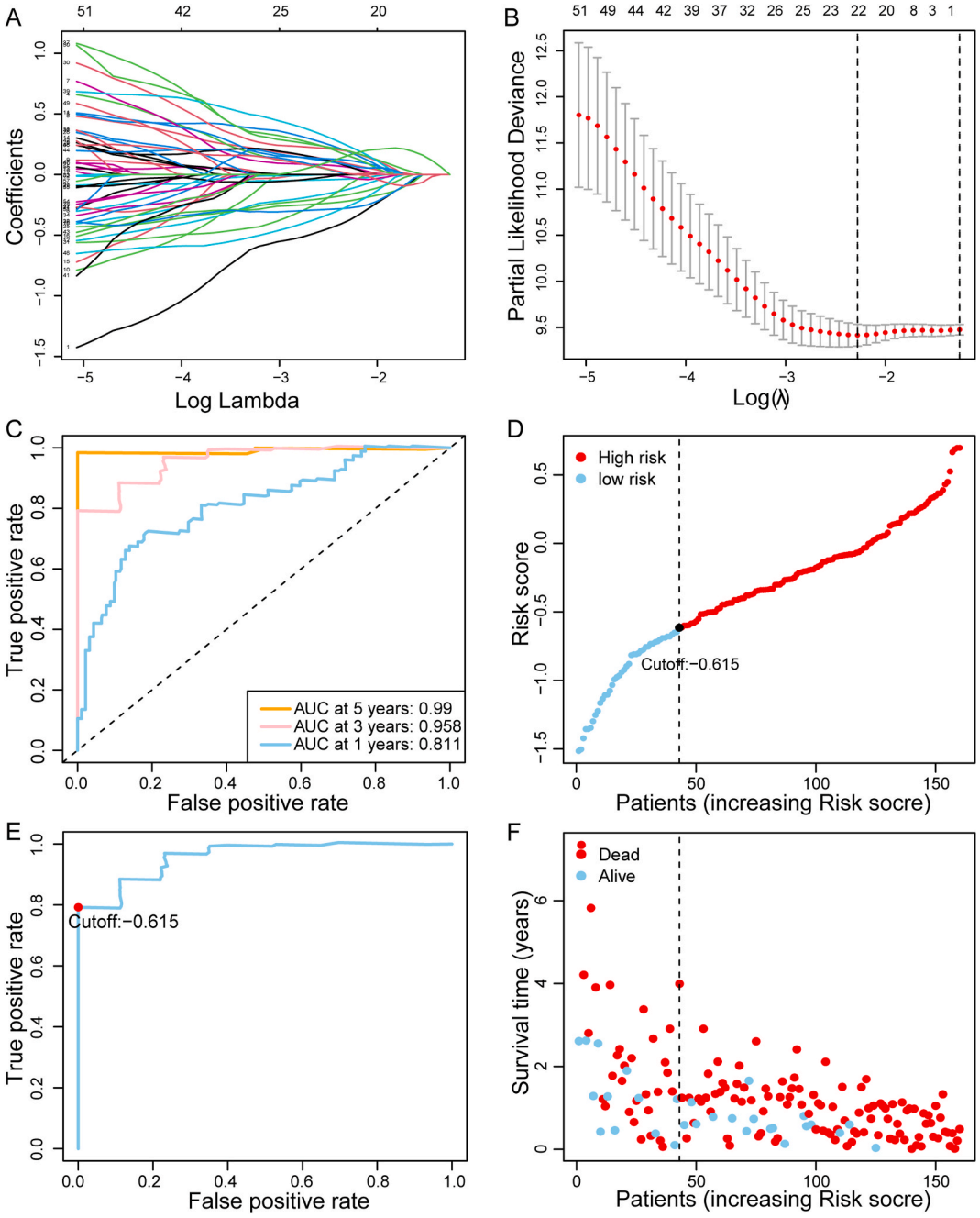

Fig. 3. Screening prognostic immune-related gene pairs (IRGPs) for model construction. (A) Lasso coefficient profiles of 22 prognostic gene pairs. (B) One thousand times random stimulation for the optimal Lasso model. (C) The AUC values for predicting 1-year, 3-year, and 5-year overall survival are 0.811, 0.958, and 0.99. (D) Patients were sorted by increasing risk score in the GBM set. (E) Time-dependent ROC curve for the risk score. The optimal cut-off value of the risk score is −0.615, and patients are divided into high- and low-risk groups. (F) Living status of patients in GBM set.

risk scores in different gender patients ($P = 0.47$, Fig. S1A), and patients with age ≤65 and age >65 ($P = 0.34$, Fig. S1B). In addition, univariate Cox model result demonstrated that radiotherapy ($P < 0.001$, HR = 0.279, 95 % CI [0.166–0.471]), age ($P = 0.024$, HR = 1.524, 95 % CI [1.057–2.169]), risk score ($P < 0.001$, HR = 8.912, 95 % CI = 5.557–14.294) were all obviously related to the OS (Fig. 4C). Moreover, multivariate Cox model results revealed that radiotherapy ($P < 0.001$, HR = 0.359, 95 % CI = 0.202–0.636) and risk score ($P < 0.001$, HR = 9.346, 95 % CI = 4.985–17.522) were independent prognostic predictors of OS (Fig. 4D).

Table 1
Information of 22 IRGPs.

Gene Pairs	Gene1	Gene2	Coefficient
AGAP2|IGHA1	AGAP2	IGHA1	−0.37389
ATCAY|DLL3	ATCAY	DLL3	0.085646
BCL2A1|LUM	BCL2A1	LUM	0.183921
C1R|HLA-DPB1	C1R	HLA-DPB1	0.059028
C5AR1|HLA-DQB1	C5AR1	HLA-DQB1	0.062105
CD163|HLA-DQB1	CD163	HLA-DQB1	0.001608
CHI3L2|HLA-DMA	CHI3L2	HLA-DMA	0.11647
CMKLR1|POSTN	CMKLR1	POSTN	−0.11862
CXCL10|LOXL1	CXCL10	LOXL1	−0.21639
CXCL11|MMP7	CXCL11	MMP7	−0.0358
DLL3|NSG2	DLL3	NSG2	−0.16289
GPC2|ZDHHC22	GPC2	ZDHHC22	0.189634
HLA-DPA1|VGF	HLA-DPA1	VGF	−0.07695
HLA-DQA1|LOXL1	HLA-DQA1	LOXL1	−0.27508
HLA-DQB1|NNAT	HLA-DQB1	NNAT	−0.02409
HLA-DRB6|RPRM	HLA-DRB6	RPRM	0.191532
IGHG1|IGLC2	IGHG1	IGLC2	0.22982
LTF|SAA1	LTF	SAA1	−0.25532
NNAT|RNASE6	NNAT	RNASE6	0.150905
NNAT|VOPP1	NNAT	VOPP1	0.075533
TACC3|ZNF488	TACC3	ZNF488	0.006009
VGF|ZDHHC22	VGF	ZDHHC22	0.161788

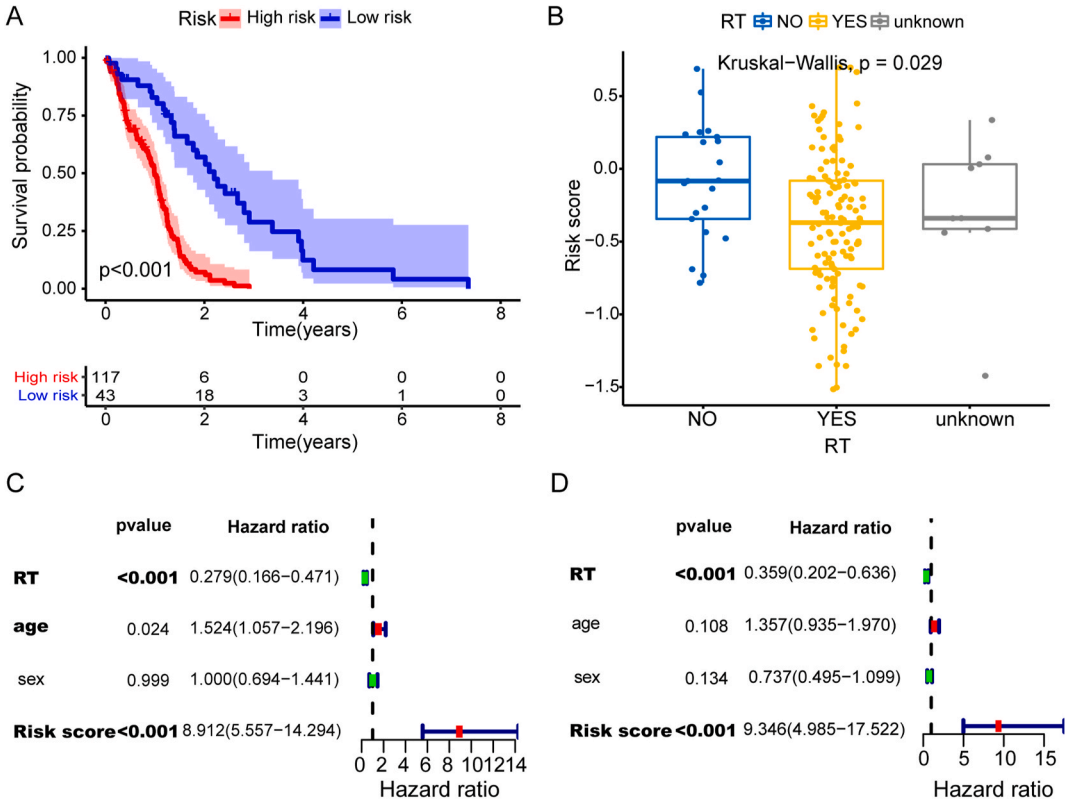

Fig. 4. Evaluate the predictive ability of the risk score. (A) Kaplan-Meier analysis shows that patients in the low-risk group experienced a longer survival time. (B) The distribution of risk score between the radiotherapy group and the non-radiotherapy group. (C) Forest plot of univariate Cox regression results of the risk score and clinical characteristics. (D) Forest plot of multivariate Cox regression results of the risk score and clinical characteristics.

3.4. Establishment and assessment of the nomogram

Subsequently, we constructed a nomogram via the risk score and radiotherapy (Fig. 5A). The C-index of the nomogram was 0.783. Calibration curves were generated to evaluate the prognostic performance of it to predict survival rates, which exhibited significant precision (Fig. 5B). In addition, decision curve analysis was used to assess the reliability of the nomogram. The result showed that the profile of the nomogram is higher compared to the limit curve, and with higher reliability (Fig. 5C).

3.5. Estimation of immune infiltration and immune checkpoints

Combined with the download data from the TIMER2.0 website, we researched the relationship between the riskscore and immune infiltration. The findings revealed a positive association with fibroblasts, macrophages, and monocytes, while a negative association was observed with B-cells (Fig. 6A). To deeply elucidate the association between the risk score and immunity, we determined its association with immune checkpoints. Our analysis demonstrated that *PDCD1* was upregulated in the high-risk group ($P = 0.0016$, Fig. 6B), whereas *LAG3* was downregulated ($P = 0.042$, Fig. S1D). Moreover, there exists an obvious positive association between the riskscore and *PDCD1* levels ($P < 0.01$, $r = 0.24$, Fig. 6C). Notably, the *PDCD1* high-expression group has a worse prognosis (Fig. 6D). Furthermore, survival analysis of patients receiving radiotherapy showed significantly better outcomes regardless of their *PDCD1* expression status. Among radiotherapy-treated patients specifically, those in the *PDCD1* high-expression group had shorter OS (Fig. 6E).

3.6. Gene set enrichment analysis

We used GSEA to investigate the molecular mechanisms associated with the risk score. The results revealed significant enrichment of multiple KEGG pathways, including cytokine-cytokine receptor interaction, ECM-receptor interaction, the Notch pathway, WNT

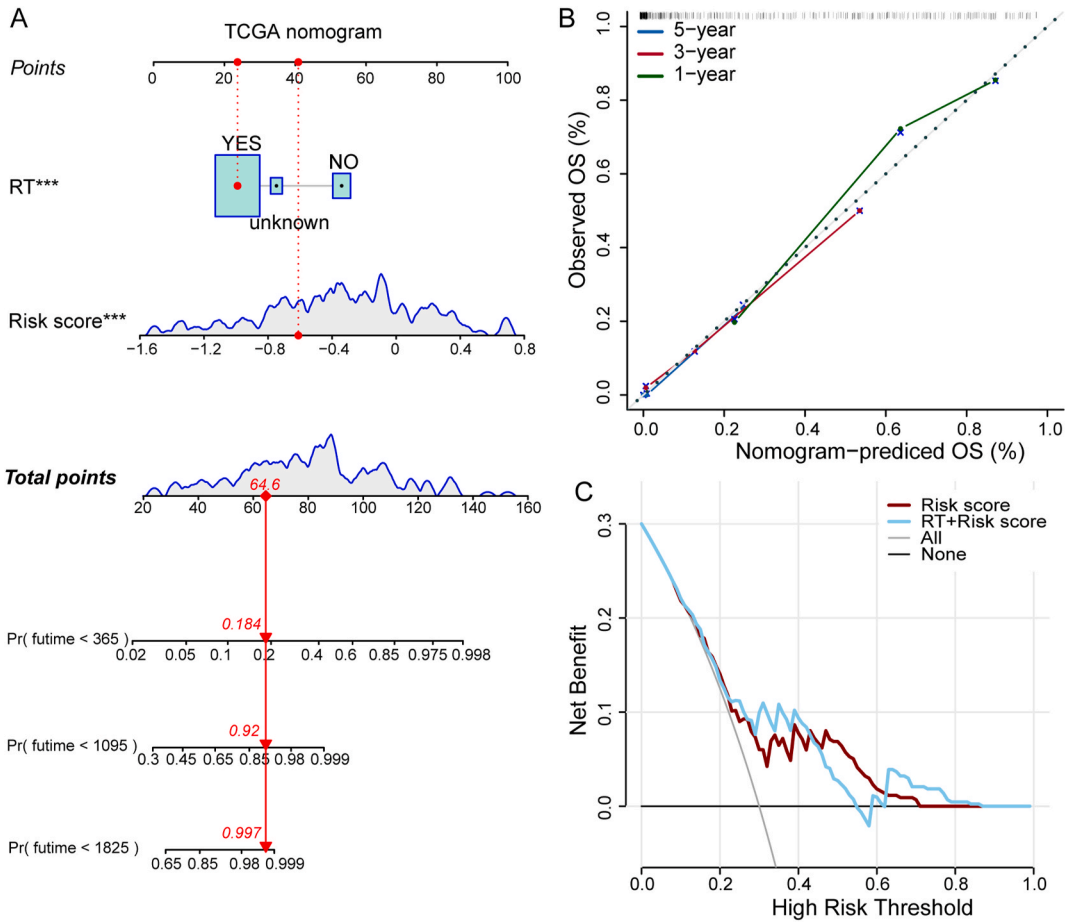

Fig. 5. Construction and evaluation of the nomogram. (A) Nomogram for predicting the survival probability based on the risk score and clinical variables. (B) The calibration plot for validation of the nomogram for 1-year, 3-year, and 5-year overall survival. The x-axis represents the predictable probability, and the y-axis represents the actual probability. (C) Decision curve analyses of the nomogram.

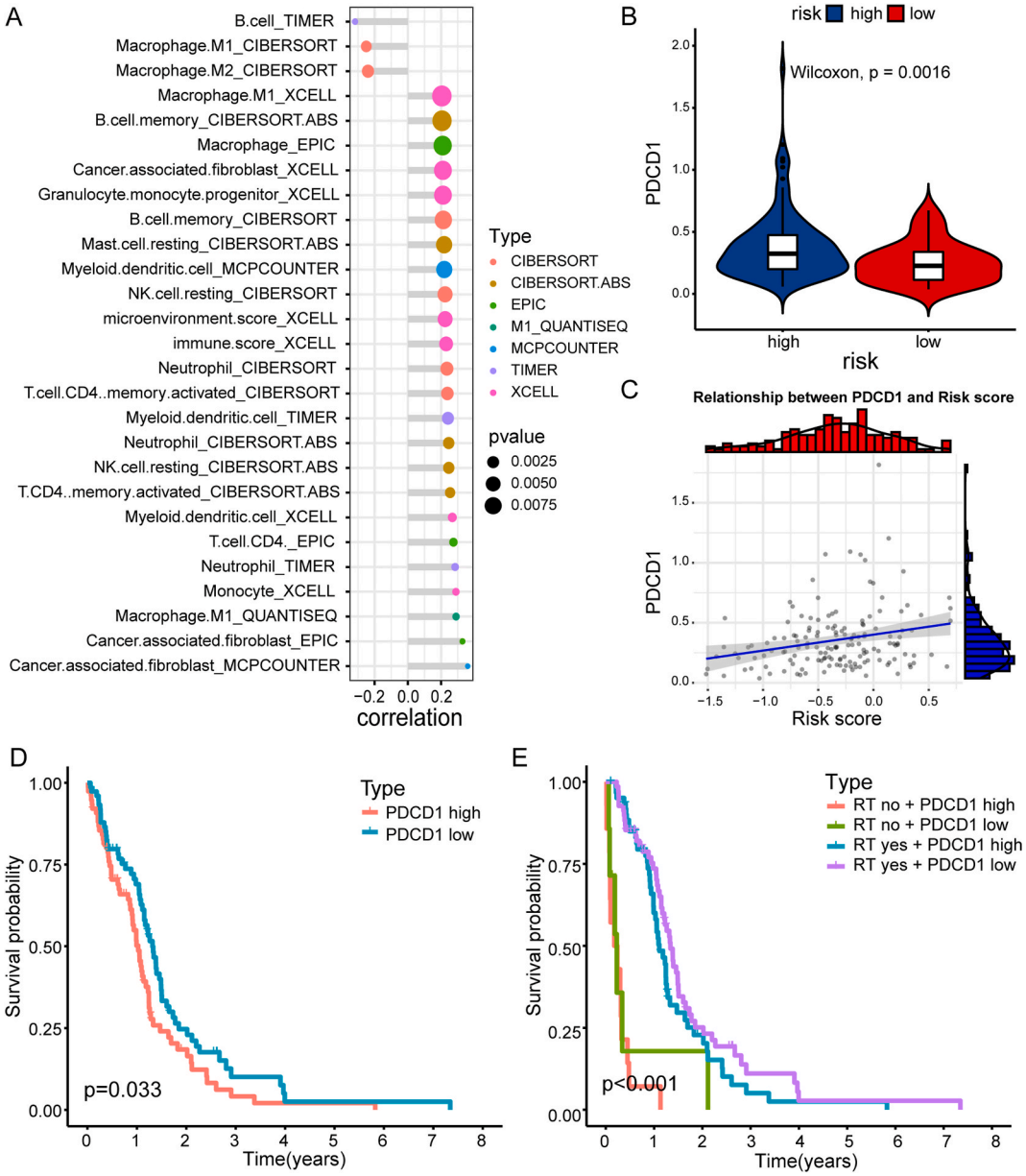

Fig. 6. Estimation of immune cell infiltration and immune checkpoints. (A) Correlation matrix between the abundance of immune cells and the risk score. (B) The differential expressions of *PDCD1* between high- and low-risk groups. (C) The association between the risk score and *PDCD1*. (D) Kaplan Meier survival analysis between high and low *PDCD1* expression groups. (E) Kaplan Meier survival analysis of radiotherapy in combination with *PDCD1* expression.

pathway (Fig. 7A). Furthermore, analysis of patient samples demonstrated enrichment of hallmarks such as IL2-STAT5, IL6-JAK-STAS3 pathway, NOTCH signaling, and Wnt/beta-catenin signaling (Fig. 7B). These significantly enriched hallmarks played a critical role in shaping the immune microenvironment.

4. Discussion

GBM is a highly malignant, invasive, and poorly prognosis brain tumor [28]. The main therapy method includes surgery, chemotherapy, and radiotherapy [29]. Besides the traditional treatments, there are no novel treatments that can be applied in clinical practice to improve the survival of GBM. Recently, immune checkpoint inhibitor (ICI) therapy, the most extensively studied immunotherapy, has displayed promising clinical efficacy in various tumors [30]. Nevertheless, for the immunosuppressive tumor microenvironment, and extensive heterogeneity, the majority of GBM patients respond to immunotherapy ineffectively [31,32]. Hence, it is

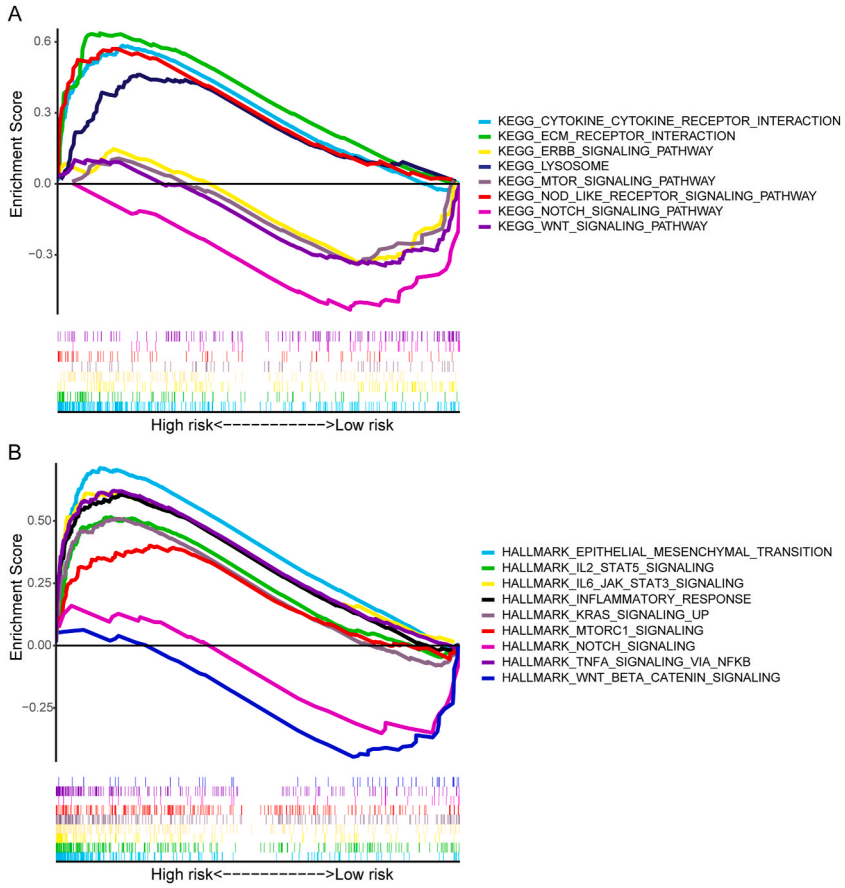

Fig. 7. Results of gene set enrichment analysis (GSEA). (A) The significantly enriched KEGG pathways by GSEA. (B) The significantly enriched Hallmarks by GSEA.

very necessary to develop new biomarkers in the therapy of GBM.

Firstly, we used ssGSEA to determine the enrichment score of the included samples and grouped samples into two immunity groups. The differential expressed genes of the high-versus low-immunity group, and normal versus tumor group were intersected. Secondly, the intersecting genes were assigned in pairs to construct the risk model. In the past, traditional prognostic models were involved in the exact expression level of genes, which are susceptible to individual variation. In our study, the pairwise comparison and score calculation are entirely based on the relative ranking of gene expression values of the same patient. Therefore, our signature can effectively overcome the bath effects and does not need data normalization. This method was robust in many solid tumors, including bladder cancer [33], colorectal cancer [34], esophageal cancer [35], ovarian cancer [36], and NSCLC [25].

Our signature includes 36 immune-related genes which are mainly related to immune cell function and antigen identification and presentation. We focus on the *CXCL10* and *CXCL11*, which are a subfamily of chemokines that are mainly involved in immune cell recruitment and participate in the pathological process of tumors [37]. *CXCL10* enhances anti-tumor immunity and transforms cold tumors into hot tumors [38]. In the tumor microenvironment, by increasing tumor-infiltrating T cells and enhancing T-cell activity, *CXCL10* can significantly limit GBM growth [39]. Li reported that *CXCL9* and *CXCL10* can be regarded as immune therapy targets [40]. Other immune-related genes in our signature are also tightly correlated with cancer [41,42]. Especially, CD163, CMKLR1, CHI3L2, POSTN, LTF, SAA1, and TACC3 et al. were associated with various phenotypes of GBM, such as radioresistance, proliferation, epithelial-mesenchymal transition, migration, invasion, apoptosis, immune infiltration, stem cell self-renewal, etc. and are significantly correlated with poor prognosis of GBM [43–51]. In addition, the riskscore exhibits high prediction performance for OS, and the AUC values to predict 1, 3, and 5-year OS are 0.811, 0.958, and 0.99, respectively. Survival and Cox analysis result confirmed that our risk score is an independent prognostic factor. It should be noted that age and sex have lower predictive values. Hence, our risk score may be more valuable in predicting the survival of GBM patients.

Moreover, the risk score was positively associated with fibroblasts, macrophages, and monocytes, while inversely related to B cells. Immune heterogeneity was observed between different risk groups. The tumor microenvironment (TME) means the surrounding environment in which tumor cells reside, including extracellular matrix, signaling molecules, immune cells, fibroblasts, lipocytes, etc. [52]. Among the multiple components of the TME, cancer-associated fibroblasts facilitate the formation of the immunosuppressive microenvironment that affects the response to immune checkpoint therapy [53]. In addition, tumor-associated macrophages (TAMs) in

the TME play a dominant role at different stages of tumor invasion and metastasis [54]. They are mainly classified into anti-tumor M1 and pro-tumor M2 subtypes, the level of which is closely related to patient survival depending upon their M1 to M2 type [55]. In addition, TAMs can inhibit the therapeutic effect of ICI through various mechanisms, such as elevating the levels of PD-1 and PD-L1 [56] and inhibiting the interaction between T cells and tumor cells [57].

In addition, the risk score was positively associated with *PD-L1* expression. Therefore, patients in the high-risk group may be more sensitive to immunotherapy. Moreover, high *PD-L1* expression predicted poor prognosis, consistent with the previous study [58]. Previous studies have shown that immunotherapy alone may not achieve a positive effect on GBM, but shows encouraging results in combination with radiotherapy [59]. Therefore, radiotherapy exerts a crucial role in the treatment of GBM patients. In our study, we observed improved survival rates in the group receiving radiotherapy combined with low expression of *PD-L1* compared to those with high expression. Therefore, we speculate that patients in low-risk group combined with radiotherapy may observe more benefits.

Finally, the molecular mechanisms associated with the risk score were explored via GSEA. The Wnt and Notch pathways were more abundant in the low-risk group. Both of these signaling pathways are evolutionarily conserved and play a critical role in carcinogenesis and the regulation of immune response [60,61]. Wnt pathway boosts the maturation and infiltration of macrophages for immune surveillance in the steady state but also polarizes TAMs toward immunosuppressive M2-like phenotypes for immune escape in the TME [62]. Another study showed that pharmacologic inhibition of Wnt signaling represents a promising method for reversing immune tolerance and improving the effect of PD-1 blockade [63]. Conversely, the ECM receptor interaction pathway was more abundant in the high-risk group. Glycosaminoglycans and proteoglycans regulate the adhesion of glioma cells to ECM protein and cause cell proliferation and migration [64]. Furthermore, we observed an extensive enrichment of immune-related hallmarks in the high-risk group.

There exist a few limitations in our research. Firstly, it is only based on bioinformatic analysis, the collection of clinical samples is needed for further validation. Secondly, due to the lack of immunotherapy data, immunotherapy combined with radiotherapy for predicting the prognosis of glioblastoma needs further research. Hence, further prospective research is needed to prove the obtained findings.

5. Conclusions

The IRGP signature can precisely predict the prognosis of patients with GBM. Additionally, the IRGP signature might help in the identification of patients who are more likely to benefit from immunotherapy.

Funding

This research was funded by the Beijing Medical Award Foundation (No.YXTL-2023-726-0158) and the Shanghai Zhenghao Charity Foundation (No.ZH-YXJK-34).

Data availability

The public data set of the present research was found in the TCGA database.

CRediT authorship contribution statement

Gang Wang: Writing – original draft, Methodology. **Yingchun Man:** Methodology. **Kui Cao:** Methodology. **Lihong Zhao:** Visualization, Validation. **Lixin Lun:** Visualization, Validation. **Yiyang Chen:** Writing – review & editing, Supervision. **Xinyu Zhao:** Supervision, Investigation. **Xueying Wang:** Supervision, Investigation. **Lijie Zhang:** Writing – review & editing, Writing – original draft, Funding acquisition, Conceptualization. **Chuncheng Hao:** Writing – review & editing, Writing – original draft, Funding acquisition, Conceptualization.

Declaration of competing interest

The authors declare that they have no known competing financial interests or personal relationships that could have appeared to influence the work reported in this paper.

Acknowledgements

We thank all the R software developers.

Appendix A. Supplementary data

Supplementary data to this article can be found online at https://doi.org/10.1016/j.heliyon.2024.e39025.

References

[1] E. Agosti, M. Zeppieri, L. De Maria, et al., Glioblastoma immunotherapy: a systematic review of the present strategies and prospects for advancements, Int. J. Mol. Sci. 24 (20) (2023).
[2] M.W. Stupp R, M.J. van den Bent, Radiotherapy plus concomitant and adjuvant temozolomide for glioblastoma, N. Engl. J. Med. 352 (10) (2005) 987–996.
[3] H.M. Stupp R, W.P. Mason, Effects of radiotherapy with concomitant and adjuvant temozolomide versus radiotherapy alone on survival in glioblastoma in a randomised phase III study: 5-year analysis of the EORTC-NCIC trial, Lancet Oncol. 10 (5) (2009) 459–466.
[4] S. Mallick, R. Benson, A. Hakim, et al., Management of glioblastoma after recurrence: a changing paradigm, J. Egypt. Natl. Cancer Inst. 28 (4) (2016) 199–210.
[5] Q.T. Ostrom, G. Cioffi, H. Gittleman, et al., CBTRUS statistical report: primary brain and other central nervous system tumors diagnosed in the United States in 2012–2016, Neuro Oncol. 21 (Supplement_5) (2019) v1–v100.
[6] T.F. Cloughesy, W.K. Cavenee, P.S. Mischel, Glioblastoma: from molecular pathology to targeted treatment, Annu. Rev. Pathol. 9 (1) (2014) 1–25.
[7] Q. Tang, Y. Chen, X. Li, et al., The role of PD-1/PD-L1 and application of immune-checkpoint inhibitors in human cancers, Front. Immunol. 13 (2022).
[8] J. Liu, Z. Chen, Y. Li, et al., PD-1/PD-L1 checkpoint inhibitors in tumor immunotherapy, Front. Pharmacol. 12 (2021).
[9] M. Yang, M. Cui, Y. Sun, et al., Mechanisms, combination therapy, and biomarkers in cancer immunotherapy resistance, Cell Commun. Signal. 22 (1) (2024).
[10] C. Robert, W.-J. Hwu, O. Hamid, et al., Long-term safety of pembrolizumab monotherapy and relationship with clinical outcome: a landmark analysis in patients with advanced melanoma, Eur. J. Cancer 144 (2021) 182–191.
[11] A. Sezer, S. Kilickap, M. Gümüş, et al., Cemiplimab monotherapy for first-line treatment of advanced non-small-cell lung cancer with PD-L1 of at least 50%: a multicentre, open-label, global, phase 3, randomised, controlled trial, Lancet 397 (10274) (2021) 592–604.
[12] D.A. Reardon, A.A. Brandes, A. Omuro, et al., Effect of nivolumab vs bevacizumab in patients with recurrent glioblastoma, JAMA Oncol. 6 (7) (2020).
[13] A.B. Heimberger, P. Sharma, J. Allison, et al., Window-of-opportunity clinical trial of pembrolizumab in patients with recurrent glioblastoma reveals predominance of immune-suppressive macrophages, Neuro Oncol. 22 (4) (2020) 539–549.
[14] M. Caccese, S. Indraccolo, V. Zagonel, et al., PD-1/PD-L1 immune-checkpoint inhibitors in glioblastoma: a concise review, Crit. Rev. Oncol. Hematol. 135 (2019) 128–134.
[15] C. Noronha, A.S. Ribeiro, R. Taipa, et al., PD-L1 tumor expression is associated with poor prognosis and systemic immunosuppression in glioblastoma, J. Neuro Oncol. 156 (3) (2022) 453–464.
[16] N. Sobhani, V. Bouchè, G. Aldegheri, et al., Analysis of PD-L1 and CD3 expression in glioblastoma patients and correlation with outcome: a single center report, Biomedicines 11 (2) (2023).
[17] L. Zhao, J. Zhang, S. Xuan, et al., Molecular and clinicopathological characterization of a prognostic immune gene signature associated with MGMT methylation in glioblastoma, Front. Cell Dev. Biol. 9 (2021).
[18] H. Qiu, Y. Li, S. Cheng, et al., A prognostic microenvironment-related immune signature via ESTIMATE (PROMISE model) predicts overall survival of patients with glioma, Front. Oncol. 10 (2020).
[19] W.Y. Wang Y, S. Wang, C. Wang, Y. Tang, C. Zhang, D. Yu, S. Hou, N. Lin, Comprehensive analysis of CYBB as a prognostic marker and therapeutic target in glioma: a bioinformatics approach, Heliyon 10 (8) (2024) e29549.
[20] Y.-L. Lan, S. Zou, B. Qin, et al., Analysis of the sodium pump subunit ATP1A3 in glioma patients: potential value in prognostic prediction and immunotherapy, Int. Immunopharm. 133 (2024).
[21] M. Cheng, L. Liu, Y. Zeng, et al., An inflammatory gene-related prognostic risk score model for prognosis and immune infiltration in glioblastoma, Mol. Carcinog. 63 (2) (2023) 326–338.
[22] Z. Qin, B. Yang, X. Jin, et al., Cuproptosis in glioblastoma: unveiling a novel prognostic model and therapeutic potential, Front. Oncol. 14 (2024).
[23] K. Wang, Y. Xiao, R. Zheng, et al., Immune cell infiltration and drug response in glioblastoma multiforme: insights from oxidative stress-related genes, Cancer Cell Int. 24 (1) (2024).
[24] Q. Bao, X. Yu, X. Qi, Integrated analysis of single-cell sequencing and weighted co-expression network identifies a novel signature based on cellular senescence-related genes to predict prognosis in glioblastoma, Environ. Toxicol. 39 (2) (2023) 643–656.
[25] B. Li, Y. Cui, M. Diehn, et al., Development and validation of an individualized immune prognostic signature in early-stage nonsquamous non–small cell lung cancer, JAMA Oncol. 3 (11) (2017).
[26] N. Simon, J. Friedman, T. Hastie, et al., Regularization paths for cox's proportional hazards model via coordinate descent, J. Stat. Software 39 (5) (2011).
[27] L.T. Heagerty Pj, M.S. Pepe, Time-dependent ROC curves for censored survival data and a diagnostic marker, Biometrics 56 (2) (2000) 337–344.
[28] I. Salvato, A. Marchini, Immunotherapeutic strategies for the treatment of glioblastoma: current challenges and future perspectives, Cancers 16 (7) (2024).
[29] A.F. Aldoghachi, A.F. Aldoghachi, K. Breyne, et al., Recent advances in the therapeutic strategies of glioblastoma multiforme, Neuroscience 491 (2022) 240–270.
[30] M. Borgeaud, J. Sandoval, M. Obeid, et al., Novel targets for immune-checkpoint inhibition in cancer, Cancer Treat Rev. (2023) 120.
[31] R. Zhao, Z. Pan, B. Li, et al., Comprehensive analysis of the tumor immune microenvironment landscape in glioblastoma reveals tumor heterogeneity and implications for prognosis and immunotherapy, Front. Immunol. 13 (2022).
[32] F. Yasinjan, Y. Xing, H. Geng, et al., Immunotherapy: a promising approach for glioma treatment, Front. Immunol. 14 (2023).
[33] Y. Fu, S. Sun, J. Bi, et al., A novel immune-related gene pair prognostic signature for predicting overall survival in bladder cancer, BMC Cancer 21 (1) (2021).
[34] B. Pan, Y. Yue, W. Ding, et al., A novel prognostic signatures based on metastasis- and immune-related gene pairs for colorectal cancer, Front. Immunol. 14 (2023).
[35] W. Zheng, G. Fang, Q. Huang, et al., A robust immune-related gene pairs signature for predicting the overall survival of esophageal cancer, BMC Genom. 24 (1) (2023).
[36] B. Zhang, X. Nie, X. Miao, et al., Development and verification of an immune-related gene pairs prognostic signature in ovarian cancer, J. Cell Mol. Med. 25 (6) (2021) 2918–2930.
[37] C. Zhou, Y. Gao, P. Ding, et al., The role of CXCL family members in different diseases, Cell Death Discovery 9 (1) (2023).
[38] N. Karin, Chemokines in the landscape of cancer immunotherapy: how they and their receptors can Be used to turn cold tumors into hot ones? Cancers 13 (24) (2021).
[39] J. Mao, J. Li, J. Chen, et al., CXCL10 and Nrf2-upregulated mesenchymal stem cells reinvigorate T lymphocytes for combating glioblastoma, Journal for ImmunoTherapy of Cancer 11 (12) (2023).
[40] Y. Li, S. Han, B. Wu, et al., CXCL11 correlates with immune infiltration and impacts patient immunotherapy efficacy: a pan-cancer analysis, Front. Immunol. 13 (2022).
[41] P.-L. Su, K. Chakravarthy, N. Furuya, et al., DLL3-guided therapies in small-cell lung cancer: from antibody-drug conjugate to precision immunotherapy and radioimmunotherapy, Mol. Cancer 23 (1) (2024).
[42] S. Dorafshan, M. Razmi, S. Safaei, et al., Periostin: biology and function in cancer, Cancer Cell Int. 22 (1) (2022).
[43] S. Yu, L. Lv, Y. Li, et al., PLK3 promotes the proneural–mesenchymal transition in glioblastoma via transcriptional regulation of C5AR1, Mol. Biol. Rep. 50 (10) (2023) 8249–8258.
[44] H. Li, D. Wang, B. Yi, et al., Comprehensive analysis of CD163 as a prognostic biomarker and associated with immune infiltration in glioblastoma multiforme, BioMed Res. Int. 2021 (2021) 1–24.
[45] J. Wu, S. Shen, T. Liu, et al., Chemerin enhances mesenchymal features of glioblastoma by establishing autocrine and paracrine networks in a CMKLR1-dependent manner, Oncogene 41 (21) (2022) 3024–3036.
[46] Y. Luan, H. Zhang, Y. Liu, et al., UTX inhibition suppresses proliferation and promotes apoptosis in patient-derived glioblastoma stem cells by modulating periostin expression, J. Cell. Physiol. 239 (4) (2024).

[47] H. Wang, L. Yao, J. Chen, et al., The dual role of POSTN in maintaining glioblastoma stem cells and the immunosuppressive phenotype of microglia in glioblastoma, J. Exp. Clin. Cancer Res. 43 (1) (2024).
[48] Y. Wang, B. Wang, W. Cao, et al., PTX3 activates POSTN and promotes the progression of glioblastoma via the MAPK/ERK signalling axis, Biochem. Biophys. Res. Commun. 703 (2024).
[49] K. Qiu, D. Ding, F. Zhang, et al., LTF as a potential prognostic and immunological biomarker in glioblastoma, Biochem. Genet. (2024).
[50] G. Cui, Y. Xiao, Identification of SAA1 as a prognostic biomarker associated with immune infiltration in glioblastoma, Autoimmunity 55 (6) (2022) 418–427.
[51] Y. Lu, Y. Shao, Multicellular biomarkers of drug resistance as promising targets for glioma precision medicine and predictors of patient survival, Cancer Drug Resistance 5 (2) (2022) 511–533.
[52] Y. Jin, Y. Huang, H. Ren, et al., Nano-enhanced immunotherapy: targeting the immunosuppressive tumor microenvironment, Biomaterials 305 (2024).
[53] H. Zhang, X. Yue, Z. Chen, et al., Define cancer-associated fibroblasts (CAFs) in the tumor microenvironment: new opportunities in cancer immunotherapy and advances in clinical trials, Mol. Cancer 22 (1) (2023).
[54] U. Basak, T. Sarkar, S. Mukherjee, et al., Tumor-associated macrophages: an effective player of the tumor microenvironment, Front. Immunol. 14 (2023).
[55] H. Wang, X. Wang, X. Zhang, et al., The promising role of tumor-associated macrophages in the treatment of cancer, Drug Resist. Updates (2024) 73.
[56] M. Lopez-Yrigoyen, L. Cassetta, J.W. Pollard, Macrophage targeting in cancer, Ann. N. Y. Acad. Sci. 1499 (1) (2020) 18–41.
[57] E. Peranzoni, E. Donnadieu, Improving efficacy of cancer immunotherapy through targeting of macrophages, Hum. Vaccines Immunother. 15 (1) (2018) 189–192.
[58] Z. Zhu, H. Zhang, B. Chen, et al., PD-L1-Mediated immunosuppression in glioblastoma is associated with the infiltration and M2-polarization of tumor-associated macrophages, Front. Immunol. 11 (2020).
[59] O.M. Ozpiskin, L. Zhang, J.J. Li, Immune targets in the tumor microenvironment treated by radiotherapy, Theranostics 9 (5) (2019) 1215–1231.
[60] P. Song, Z. Gao, Y. Bao, et al., Wnt/β-catenin signaling pathway in carcinogenesis and cancer therapy, J. Hematol. Oncol. 17 (1) (2024).
[61] M. Wang, F. Yu, Y. Zhang, et al., Novel insights into Notch signaling in tumor immunity: potential targets for cancer immunotherapy, Front. Immunol. 15 (2024).
[62] Y. Yuan, D. Wu, Y. Hou, et al., Wnt signaling: modulating tumor-associated macrophages and related immunotherapeutic insights, Biochem. Pharmacol. 223 (2024).
[63] N.C. DeVito, M. Sturdivant, B. Thievanthiran, et al., Pharmacological Wnt ligand inhibition overcomes key tumor-mediated resistance pathways to anti-PD-1 immunotherapy, Cell Rep. 35 (5) (2021).
[64] C.B.N. Mendes de Aguiar, B. Lobão-Soares, M. Alvarez-Silva, et al., Glycosaminoglycans modulate C6 glioma cell adhesion to extracellular matrix components and alter cell proliferation and cell migration, BMC Cell Biol. 6 (1) (2005).